7th International Conference
"New Horizons Towards Sustainable Development"
6-7 November 2023, Dina Al-Maadawi Hotel, Egypt
International Journal of Environmental Studies and Researches (2023), 2 (4):176-211

Preparation and Characterization of Organic Nanometric Materials for Industria Wastewater Treatment

Ahmed M. Zayed[1], Sameh A. Rizk[2], Ali H. Saleh[1], Mohamed F. Azazy[1]

[1]Environmental Studies and Research Institute, University of Sadat City
[2]Chemistry Department, Faculty of Science, Ain Shams University, Cairo 11566, Egypt

Abstract

Materials haven't currently been prevented in existing regulations for the water quality areas are considered as emerging pollutants. Organophosphorus insecticides and pharmaceutical residues are two groups of emerging pollutants having devastating impact on environment and water systems. In this study, the authors efficiently created the hydrochar (biowaste banana peels source) burdened with titanium nanoparticles (HC-TiNPs) via a microwave-Ultrasonic assisted (an efficient green as ecofriendly environment technique) hydrothermal method. Such created material was branded and evaluated for removing harmfully significant pesticides e.g., Diazinon (DIA), Terbufos (TER) and Ethoprophos (ETH), combined with four pharmaceutical compounds e.g., Paracetamol (PAR), Ketoprofen (KET), Diclofenac (DIC) and Ibuprofen (IBU) from aqueous solutions. DFT study be computed the stability of MOF and its powerful to absorb the chemical residues. It indicated the optimized structures outlined the strong adsorption due to negative charge transfer from MOF to the insecticide or pharmaceutical pollutants. The surface textural and morphological structures of as-obtained composite were determined using different analytical tools. The influence of various parameters, including adsorbent dosage (35-75 mg), initial concentration (0.1-1.2 mg/L), incubation time (25-55 min) and pH (4-8) can be determined for both insecticide and pharmaceutical. Under these conditions, HC-TiNPs was efficiently used to remove insecticide and pharmaceuticals from ecological water samples.

Keywords: Microwave-Ultrasonic (MW/US), DFT, Emerging, Hydrochar, Adsorption, Insecticides, Pharmaceuticals, Water treatment.

Introduction

Water is the main life's need on earth, being considered an essential constituent for all forms of lives, from man to micro-organism and environment especially in Egypt **(Yu et al., 2019)**. The unplanned urbanization with increasing growing population and wide sphere of human activities have brought a greater stress on surface and groundwater, which in turn results in a steady increase in the demand for water resources. Water resources, mostly are suffering from the pollution via direct and indirect channel in sanitary drainage from villages, industrial plants and located cities on these water sequences as stated by **(Palamuleni and Akoth 2015)**. Given that location is the dry sash region, Egypt depends on the Nile as its main source of water and measured now limited water resources. Extra resources providing 4% only from the total resources are considered as water challenges facing Egypt **(Elsayed et al. 2022)**. On the other hand, the most important challenge in Egypt is due to population growth without expatriates abroad. The related water demand for public water supply and economic activities, in particular, agriculture, is considered a big problem. Total amount of predictable fresh water is about 70 billion m^3 per year (Bm^3/y) **(Song et al., 2018)**. Really, we must full control water resources steadily. Water quality management, water pollution control and environmental protection are the main national goals to save our future in Egypt **(Mohamed and Rashad 2012)**. The hydrochar (HC) materials have been widely used and have been studied as eco-friendly adsorbents in water treatment. Physicochemical characterization of chars is approving the effective removal the emerging contaminants in water e.g., agrochemicals, pharmaceutically active compounds, and endocrine disrupting compounds **(Nassar et al., 2023)**. Moreover, using the low cost e.g. hydrochar (HC) be high-value carbon-rich biomass products prepared via conventional techniques instead tonot economically viable gasification, pyrolysis and flash carbonization at above 860 °C that have highly energy-intensive and 30MPa pressure **(Kumar et al., 2020)**. The microwave HTC is considered conventional method in the HC production and liquid with small amount gaseous carbon deficient products within improved preserved energy **(Hasham et al., 2021)**. Until now, there are some short-comings of conventional techniques i.e. Feedstock is heated under fairly high pressure in the presence catalyst afforded unwanted side reactions causing lower yield **(Shao et al., 2019)**. So, in the present work the authors introduced controlled condition of the process no longer residence times with nano concentration to make desired products**.** In wastewater treatment application, a variety of efficient, eco-friendly and cost-effective nano-materials have been developed having unique functionalities for potential decontamination of industrial effluents, surface water, ground water and drinking water **(Gupta et al., 2015)**. This can be achieved either by development of completely new methods or by improving the existing methods through some interventions. Among the various emerging technologies, the advancement in nanotechnology has proved an incredible potential for the remediation of wastewater and various other environmental problems **(Zare et al., 2013)**. Nano-adsorbent can be produced using the atoms of those elements which are chemically active and have high adsorption capacity on the surface of the nano-material **(Kyzas and Matis, 2015)**. The used materials for development of nano-adsorbents include activated

carbon, silica, clay materials, metal oxides and modified compounds in the form of composites **(El-Saliby et al., 2008)**. The nanomaterials such as metal oxides and semiconductors have gained a considerable attention of the scientists in developing wastewater treatment technologies. Diverse types of nano-catalysts are employed for degradation of pollutants in wastewater, for instance, electrocatalysts **(Dutta et al., 2014)**. Nano-adsorbents are broadly classified into various groups based on their role in adsorption process. It includes metallic nano-particles, nano structured mixed oxides, magnetic NPs and metallic oxide NPs. Factors controlling the nano-adsorbents properties are size, surface chemistry, agglomeration state, shape and fractal dimension, chemical composition, crystal structure and solubility **(OECD et al., 2010)**. Chemical activity and fine grain size are two key properties of nano-particles that make its prominent as compared to other substances such as normal scale titanium dioxide and alumina **(Kalfa et al., 2009 and Zhang et al., 2008)**. Moreover, modification in nano-particles can be carried out by some reagent to enhance its properties for metals ions pre concentration **(Khajeh and Sanchooli, 2011and Khajeh, 2010)**.

Materials and methods

The present study was done through the research plan of the National Water Research Center (NWRC) at El-Kanater El-Khyria in order to study attractive hydrocarbon material in treatment of some Emerging pollutants and physico-chemical parameters in surface water samples of drainage network. Therefore, the data are used to investigate occurrence and removal of toxic organic pollutants along El-Moheet drain.

Study area Description

In Egypt, Nile River is main source for fresh water. It drifts downstream from High Dam inAswan,Delta Barrage northward for about 950 km, where it is separated into two branches, Damietta and Rosetta that helps to a wide range of functions including agricultural, industrial and domestic water supply, fisheries and regeneration. It is problem in the Rosetta branch accepts high organic compounds concentrations, micronutrients and oil & grease (Fig. 1) **(Yu et al., 2019 and El-Sayed et al., 2022)**.

Physico-Chemical Parameter

Temperature (^{o}C)

Water Temperature checked and measured in the laboratory using a calibrated thermometer **(Abinandan et al., 2014)**.

Fig. 1. Nile River of Delta Map with Damietta and Rosetta branches.

Hydrogen Ion Concentration (pH)

The collected samples of water can be determined by the use of pH/ISE meter bench-top, InoLab equipped with WTW-720 Model SenTix41 pH combination electrode with built-in temperature sensor and calibrated using 4, 7 and 10 pH buffers (**Abinandan et al. 2014)**.

Electrical Conductivity (EC)

Measuring of ion concentration in water means an indirect measure the water ability to conduct an electrical current. The more electricity can be conducted by the water when its more ions present. It is particularly sensitive to variations in dissolved solids. The electrical conductivity was measured the water samples at standard temperature 20^{o}C using WTW Model inoLab. Conductivity, 7110 (0.0 µS/cm to 500 mS/cm); Laboratory Bench Conductivity Meter with Tetra Con 325; electrode conductivity cell on epoxy shaft, with built-in temperature, Conductivity solution and Calibration with 0.01 molKCl **(Abinandan et al., 2014)**.

Total Dissolved Salts (TDS)

Total dissolved salts are an indicator of non-point source pollution problems. It is a measure the particulate salts amount in solution associated with various land use practices i.e., TDS was measured by using the land use practices. The total dissolved solids in the water samples were determined via gravimetrical analysis **(Thongbunrod & Chaiprasert, 2021)**.

Dissolved Oxygen (DO)

DO in mg/l was measured using profiline dissolved oxygen meter, WTW Oxi 597 with a dissolved oxygen probe cell Ox 325 and self-stirring dissolved oxygen probe, stir OXG as evidenced by **Abinandan et al. (2014)**.

Total suspended salts (TSS)

Total suspended solids were strong minded in residue from 100 ml sample of water and then evaporate to dryness at 105^{o}C using the evaporating porcelain dishes and oven model HI-9321 and weighing the dried residue **(Abinandan et al., 2014)**.

Inorganic Chemical Parameters

Ammonia

Colorimetric determination of ammonia (NH_4OH) was achieved using Nessler solution **(Abinandan et al., 2014).**

Total Alkalinity

Total alkalinity was determined by electrometric titration for samples of water aliquot with a standard solution $2*10^{-2}$ N H_2SO_4), the end-point is determined with a PH-meter. While (CO^{-2}_3) carbonates and bicarbonates (HCO_3^-) detected by titration method via 2 $x10^{-2}$ N H_2SO_4 with M.O as indicators. Total alkalinity was calculated by summation of carbonate and bicarbonate and recorded as mg/l according to **Abinandan et al. (2014)**.

Major Anions

Major anions Cl^-, SO_4^{--}), and NO_3^- were strongminded in samples of water by ion chromatography (IC) (APHA, 2017). The IC has the following detection limits for anions, which indicates the sensitivity of the instrument (Table 1).

Major Cations and Trace Elements

Major cations Na^+, Mg^{+2} and Ca^{+2} trace elements Zn, Cd, Co, Ti, Cr, Cu, Pb, Mn, Ni and Al were measured by Induct Plasma- Coupled Emission Spec. (ICP-OES) with Nebulizer Ultrasonic. This Nebulizer diminishes the detection instrument limits by 10% using Perkin Elmer ICP. The samples were filtered via pore size membrane 0.45 μm **(APHA, 2017)**.

Table 1. IC Instrument's Detection Limits for Anions.

Anion	Detection limit (DL mg./l)
Chloride, Cl^- and Nitrate, NO_3^-	<0.1
Sulphate - $SO4^{-2}$	<0.5

Chemicals and standards

All used chemicals were analytical grade in the study, including titanium (IV) dioxide (TiO_2, 99%), hydrochloric acid (HCl, 32%), anhydrous sodium hydroxide (NaOH, 70%), nitric acid (HNO_3, 64%) were obtained from Merck Co. Pesticide extract with methylene chloride (CH_2Cl_2) and n-hexane and Organophosphorus standard mixture was delivered by Accu-Standard, Inc. (USA). Synthesis of solution and preparation banana peels was obtained from the local market with deionized water (DI).

HCs bio-adsorbent preparation

Hydrothermal treatment thru rinsed and oven-dried banana peels at 95°C for 185 min then crushed in a ball mill and sieved to select the particle sizes less than 0.99 mm. Added 100 mL DI for each 10 g Feed stock and the reaction mixture was heated in the microwave-ultrasonic with temperature wide-ranging 190-230°C at 0.5-3 h. The solid obtained HC was filtered using 0.45 μm filter paper, washed by DI water to eliminate water-soluble volatile matter, and oven-dried at 100°C for 2 h using a drying oven **(Zare et al., 2016)**. The HC yield was calculated as follows:

$$Yield\ (\%) = \frac{W_2}{W_1} \times 100 \qquad (1)$$

Where W_1 represents the dry weight banana peel and W_2 represents the HC weight. To determine the HC's ash content, a sample of dry HC was burned at 550°C for 3 h in the a tube furnace in air atmosphere, then the remaining ash W_{Ash} (g) was weight and the ash content calculated according to the following equation:

$$Ash\ content\% = \frac{W_{Ash}}{W_2} x100 \qquad (2)$$

Green synthesis TiNPs-banana peels HC

In a clean sanitized Erlenmeyer flask, 100 mL (0.5 M $TiCl_3$) was added to 100 mL (0.1 W/V *C. sinensis* leaves extract), which previously prepared by boiling 10 g of *C. sinensis* leaves in 100 mL of deionized water at 90 °C for 5 min. There was an instant color change from dark yellow into dark black indicating successful biosynthesis TiNPs **(Tondera et al., 2018)**. This black solution (TiNPs) was subsequently utilized as HTC media for production HC loaded titanium nanoparticles. Simply, ten gm of as-prepared banana peels bio-adsorbent is mixed with 100 mL of prepared black solution (TiNPs) and put in a Teflon sealed stainless steel reactor and heated at 180°C for 1 h in a microwave with ultrasonic as optimum conditions. After cooling down to room temperature, the aqueous solution was filtered and the obtained HC loaded TiNPs was dried at 90 °C for 2 h as outlined in Fig. 2 **(Alotaibi et al., 2024 and Alhalafi et al., 2024)**.

Fig. 2. Outline preparation methods of the hydrochar/TiO_2.

Characterization

FTIR

For the characterization of surface functional groups, The functional group of the Feed stock, is Hydrochar, (FTIR) of HC-TiNPs has been recorded on a Bruker, wave number at range from 4000 to 400 cm^{-1}.

Electron Scanning Microscopy (SEM)

Electron scanning microscope (SEM, QUANTA TIG250) was used to evaluate the surface morphologies, and elementary composition was identified with an X-ray energy dispersive spectrometer (EDX) and EDX measurements were occurred for each particle.

BET surface area%

The BET determines pore volumes, specific surface areas and average pore diameters of the green synthesized HCs be measured via N_2 adsorption isotherms at 80 K using a gas sorption analyzer. The pretreatment of degassing samples before measurement comprised under a high vacuum for 9 hrs at 195°C.

X-ray diffraction (XRD)

The XRD for HC-TiNPs crystal structures patterns was attained using X-ray diffractometer model PW/103 (an advanced diffract meter) equipped with K-Cu source of radiation (0.16 nm). The diffraction [°2θ] in range 4°–60° using fixed time with interval 0.02s. The patterns were progressed with Cu-Ni filtered radiation ($\boldsymbol{\lambda}$= 1.451023˚A) at 39 kV and 38 mA.

Magnetic characteristics

Specific magnetization (M) of HC-TiNPs curve as a function of applied magnetic field (G), was measured via a magnetometer vibrating sample **(LakeShore-7407, USA)**.

Adsorption studies

Adsorption experiments and analytical procedure

Three OPPs Terbufos (TER), Ethoprophos (ETH), Diazinon (DIA)), and four pharmaceuticals KetoproTin (KETO), Paracetamol (PARA), DicloTinac (DIC), IbuproTin (IBU)) was achieved in adsorption batch experiments using a thermostatic multifunction water bath shaker. Take known weight HC into 100 mL with known concentration (C_0) of OPPs in a 250 mL. Adjust pH of the solutions via 0.1 M of HCland NaOH. After 3 hr to complete adsorption, filter to separate the HC and residual pesticides that extracted with EPA 508. Using Gas chromatography (GC) to determine the concentrations (C_e) of each insecticide, and liquid chromatography (LC) used for pharmaceuticals. Study the adsorption isotherms at 30-180 min, 0.3-2.5 mg/L atpH 4-8 and 30-50°C. The efficiency removal and capacity of adsorption computed using the following equations:

$$\%\, Removal = \frac{(C_0 - C_e)}{C_0} \times 100 \quad (3)$$

$$q_e = \frac{(C_0 - C_e)V}{W} \quad (4)$$

where initial conc. Expressed C_0 and equilibrium concentrations(mg/L). The adsorbed amount of insecticides q_e(mg/g) at equilibrium, expressed by solution volume V(L) and the adsorbent mass W(g). Gas chromatography coupled with mass spectrometer was used to quantify the remaining pollutants concentrations after adsorption. Separation was performed on capillary column (0.25 μm, 30 m, 0.25). Programmed oven at 40-200°C/mi with GC parameters: split 15:1, 15 psi flow constant, injection volume0.5μL and injection temperature 300°C.

Adsorption kinetics

Studying the adsorption kinetics is valuable for understanding the elaborate mechanisms for the design of upcoming large scale adsorption facilities. Four kinetic models, including 1st order and 2nd order, intraparticle diffusion Weber-Morris model and kinetic Elovich model can be applied to predict the rate of adsorption and controlling mechanism of the studied insecticides and pharmaceuticals on HC **(Wang et al., 2011).** The linearized forms of four kinetic models have been implemented.

Results and discussion

Chemistry

Mechanism of MOF for water treatment

Reaction of metallic organic framework (MOF) with insecticide and pharmaceutical precursors is via adsorption process. Two types of adsorptions have functional applied either physic sorption or chemisorption. The (TiNPs) can be prepared via microwave ultrasonic reaction condition **(Alotaibi et al., 2024 and Alhalafi et al., 2024)**. Physico adsorption is thru hydrogen bond, dipole and van der waals interaction. Adsorption process is characterized simpler, efficient, low cost and energy saving. In the present work, we introduce the main target of this study is using hydrochar produced from banana peels combined with titanium dioxide nanoparticle in removal of two types of Emerging pollutants e.g., three pesticides compounds and four pharmaceutical compounds (see more in Fig. 3 outline the chemical structures of them).

Routes to make Biomaterials from agriculture wastes

1. Valorization or Recycling to bio waste material
2. Eco-friendly technologies to avoid negative effects on environment, human health, and natural water resources.
3. Large amount of agriculture wastes derived from plant byproducts.

Adsorption mechanism pesticides removable using hydrochar HC materials

Due to heterogeneous HC structure permits to remove organic pollutants from water through various adsorption mechanisms e.g., physical adsorption, and pore filling **(Nassar et al., 2023)**.

The efficiency of adsorption is controlled by several factors, such as the pH, concentration, and the organic pollutant polarity. Electrostatic interactions in between pollutants and the surface charged of HC. The adsorption efficiency can be affected by the ionic strength and pH **(Hamza et al., 2023)**. Organic adsorption contaminants onto char using the mechanism of pore filling depends on organic pollutant polarity and the nature, type, volume of total micropores and mesopores of the char. Adsorption of aromatic contaminants exclusively in the presence of functional groups occurred via the electron acceptor-donor interaction mechanism on chars which is affected by temperature **(Alotaibi et al., 2024)**. The

mechanism of adsorption via hydrophobic interactions due to their highly hydrophobic pollutant nature show a greater affinity for pollutant binding at high temperatures. The adsorption of pollutants from water in general, by HC depends on the characteristics of both pollutants and adsorbents and process conditions, involving various mechanisms hydrogen bonding, π–π interactions and pore filling, with the surface of the char are the possible mechanisms for emerging pollutant removal as in Fig. 4 **(Shalaby et al., 2024)**. The pesticides removal (e.g., diazinone, ethoprofos, etc.) from water by using hydrochar has shown of 1229 and 681 mg/kg, values respectively showed up to 64% removal from water.

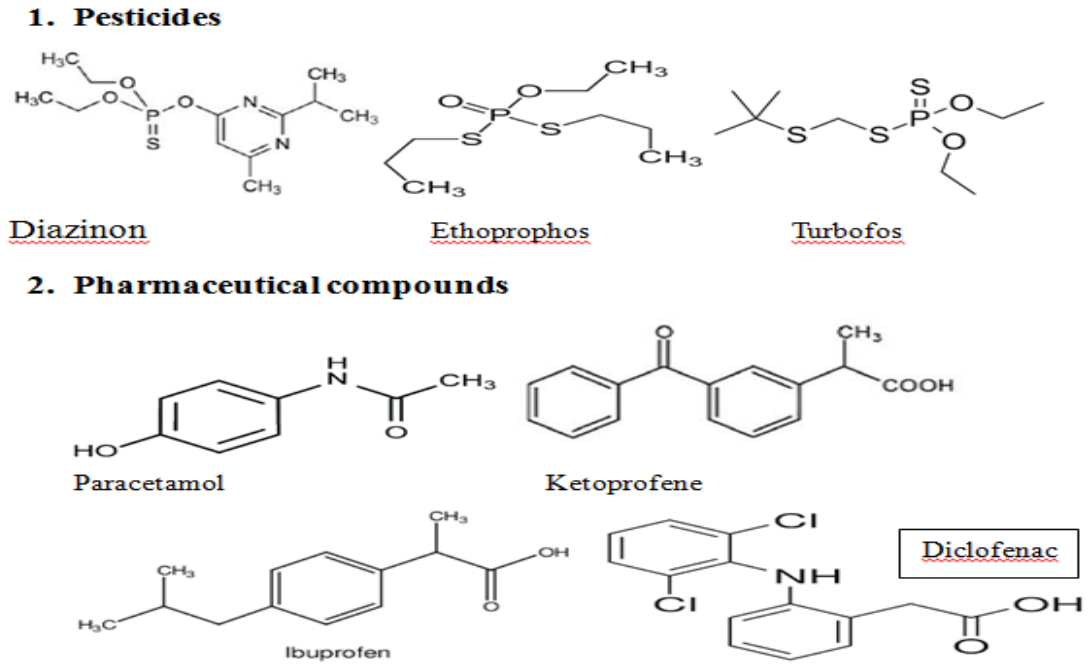

Fig. 3. Outline the chemical structures for Emerging pollutants.

Selectivity of hydrochar for organic pharmaceutical compounds in wastewaters can be ascribed to its functional groups, porous structure, electrostatic interactions, hydrochar surface, pollutant aromaticity, and the potential affinity of hydrochar. Moreover, hydrochar modifications surface can enhance its selectivity and become as a selective adsorbent for pharmaceutical compounds in water treatment.

The sustainability adsorbent of hydrochar can be elevated from its ability to be resulting from a variety of biomass as agricultural by products solid waste. Moreover, the hydrochar production of can be given bioenergy processes e.g., biodiesel production and it can be regenerated for new adsorbent materials [30]. So, the hydrochar as considered a sustainable adsorbent represents a promising development in the water land and wastewater treatment as a low cost effective and friendly environmental material.

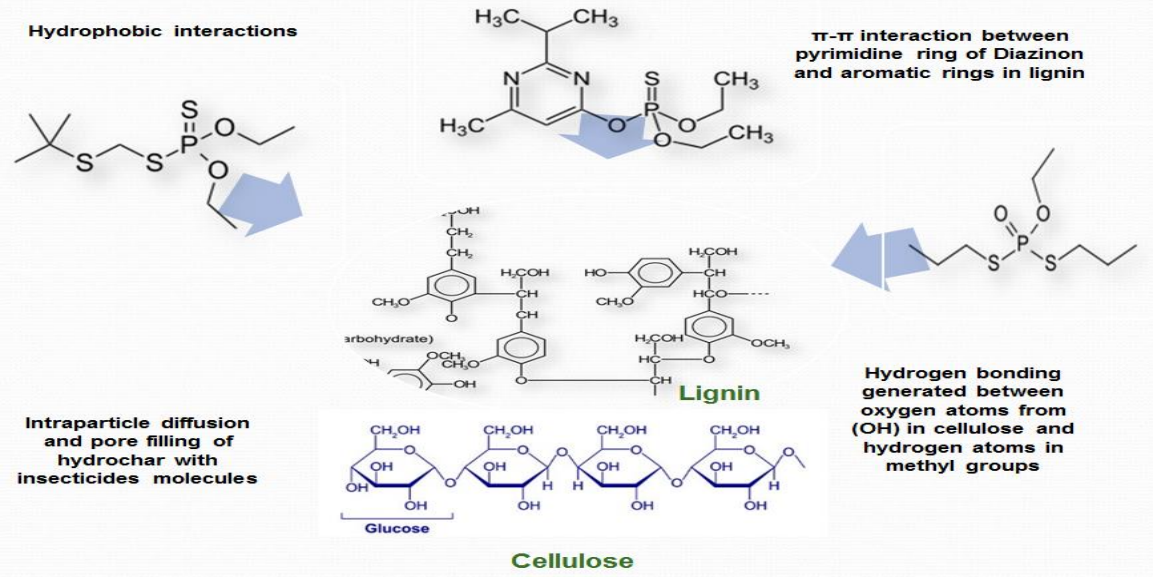

Fig. 4. Outline functional groups interaction and physical adsorption of pesticide upon lignin and cellulose in the hydrochar

DFT Study

The quantum chemical computation with density functional theory (DFT) method used for the calculations of the reaction of MOF to afford a stimulated structure that is in good agreement with the FT-IR. The listed results outlined in Table 2 indicate that the values of gap energy (ΔE), where ΔE = E_{LUMO} - E_{HOMO}. Compounds having small ΔE values are normally referred to as soft compounds, that are more reactive towards pesticide surface interactions; being capable of donating electrons via oxygen atoms in linker easily to hole surface of TiO_2 **(Hamza et al., 2024 and Rizk et al., 2024**). The removal of pesticide towards MOF-Ti is not only depended upon E_{HOMO} values, but also the number of oxygen atoms, electron distributions, surface area and lipophilicity in MOF must be considered c.f. (Table 2). The dipole moment, softness (σ, eV^{-1}) and surface area (nm^2) for most potent MOF carrying hydrophobic groups were agreed an excellent correlation between adsorption efficiency from linker to Ti ions and its back donation.

Moreover, the adsorption energy, *E*ads was then calculated using Eq. (1).

$$E\text{ads} = E(\text{HEP}) - E(\text{H}) - E(\text{EP}) \qquad \text{Eq. (1)}$$

Where $E_{(HEP)}$ is the electronic energy of the adsorbed MOF of hydrochar and emerging pollutants, $E_{(H)}$ is the electronic energy of the optimized MOF of hydrochar in vacuum, and $E_{(EP)}$ is the electronic energy of the pesticide or pharmaceutical compounds.The authors studied the adsorption properties of emerging pollutants on MOF facet using DFT methods.

Table 2. Global reactivity indices and energy level distribution of frontier orbitals.

Compound	E_{HOMO}	E_{LUMO}	ΔE(eV)	I^a	A^b	μ^c	η^d	ω^e	ΔN^f	S^g	A_{molec}(nm^2)
Hydrochar	-14.26	-14.82	0.56	12.54	12.42	4.65	1.45	26.43	0.067	0.93	599.099
diazinon	-8.99	-1.24	7.75	8.87	1.23	6.63	2.32	55.32	0.35	0.084	243.422
Paracetamol	-7.64	-2.65	5.01	7.55	2.57	5.93	3.82	49.76	0.52	0.11	230.758
Hydrochar + diazinon	-10.63	-10.78	0.15	12.00	11.98	3.61	1.43	34.82	0.077	0.93	687.625
Hydrochar + paracetamol	-9.45	-9.19	0.26	9.65	9.23	2.93	2.01	29.76	0.065	0.86	653.749

[a]Ionization potential, [b] Electron affinity, [c] Chemical potential, [d] Hardness, [e] Electrophilicityindex, [f] ucleophilicity index, [g] Softness.

First, the geometrical structure of one unit for MOF is optimized (see Fig. 5. for the optimized structure of MOF and diazinone). Then the optimized structures of insecticide is located on the MOF are indicated strong adsorption due to negative charge transfer from MOF to 2,4,5-Trichlorophenyl acetic acid.

Also, from equation (1) the Eads would be –ve value be guaranteed the influential dynamic adsorption of prepared MOF with insecticide that be good agreement with experimental value and chemical computational analysis.

Drainage water characterization

Physico-chemical parameter

Temperature (ºC)

The values of surface water temperatures for the study area recorded in Fig. 6 and Table 3 showed temperatures were in normal ranges of 17.0-35.0ºC and 26.0–36.0ºC during winter and summer seasons, respectively.

Hydrogen Ion Concentration (pH)

Samples of water are usually somewhat alkaline due to presence of $CO_3^{2-}$and HCO_3^-. The values of pH of water samples demonstrated variation values of pH that ranged from 7.7 to 8.23 and 7.63 to 7.9 during the winter and summer seasons, respectively are given in Table 3 and Fig. 7. The values of pH drainage water samples vary between 7.63 and 9.23 that are within limit of Decision 92/2013 of environmental law 48/ 1982**.**

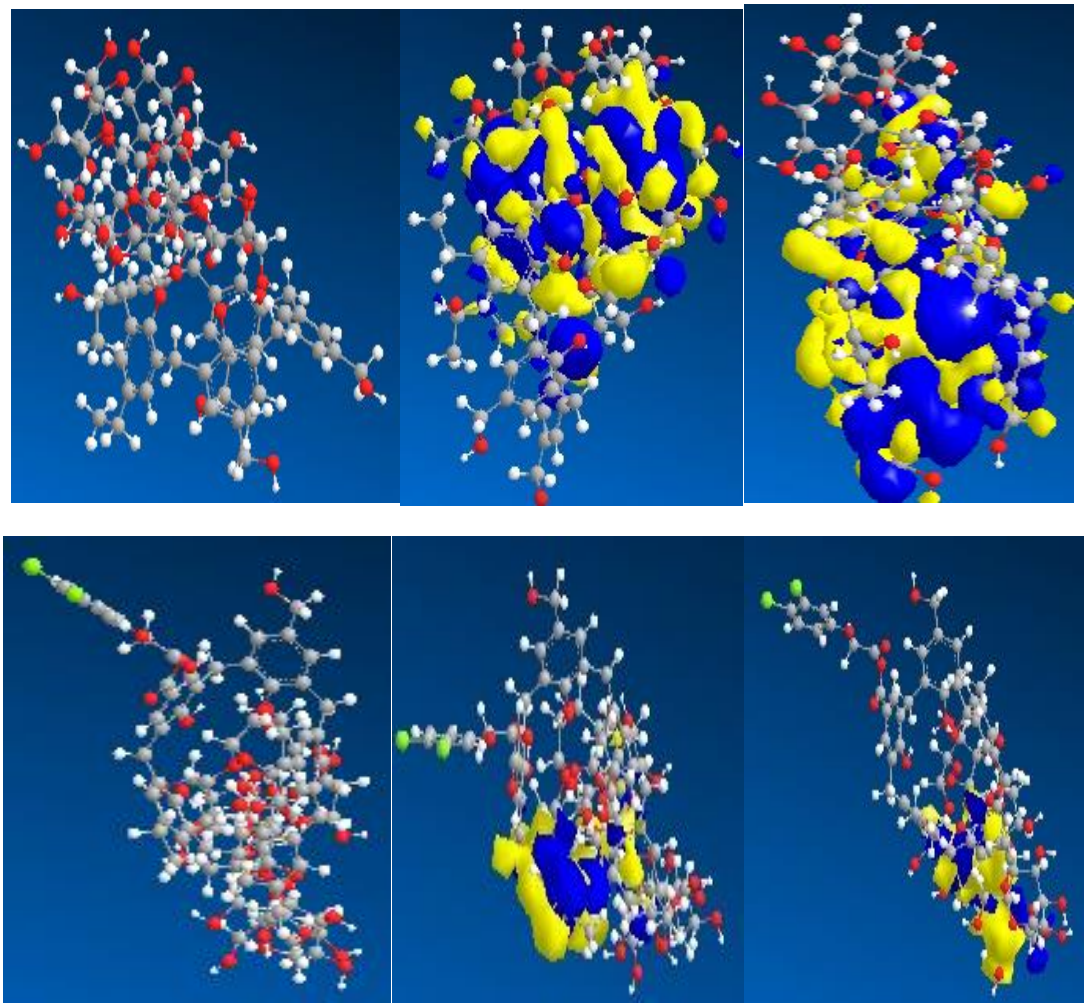

Fig. 5. Outline the optimized structures for the hydrochar and with bioadsorbent.

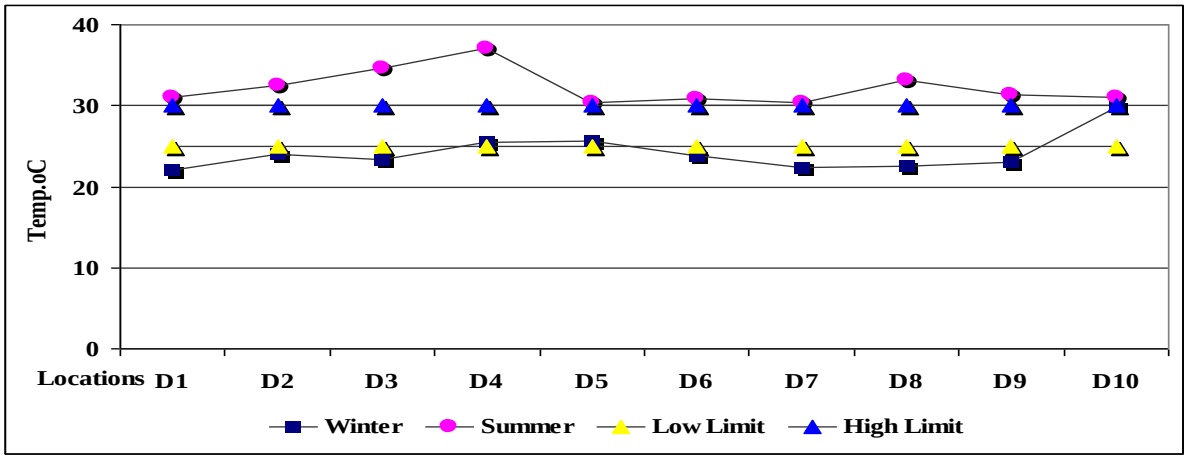

Fig. 6. Seasonal Variations of Temp. for Drainage Water Samples along El-Moheet Drain.

Table 3. Records of Physical Parameters for Water Samples DuringWinter and Summer Seasons.

Parameter	Unit	D1	D2	D3	D4	D5	D6	D7	D8	D9	D10
						Sites (Winter Season)					
Temp.	°C	22	24	23.3	25.5	25.7	23.8	22.4	22.5	23.1	29.8
pH	---	7.7	7.88	7.9	8.0	7.9	7.8	7.88	8.1	7.77	8.23
EC	dS/m	1.25	0.856	0.748	0.962	1.32	0.952	0.85	0.921	1.355	1.85
TDS	mg/l	975	548	429	433	734	496	544	590	830	840
DO	mg/l	4.6	1.9	5.24	4.97	4.89	2.97	2.31	2.71	1.86	1.54
Turbidity	NTU	13.4	29.6	5.1	11.4	15.9	27.1	8.5	10.9	12.2	18.6
TSS	mg/l	113.4	329.6	45.1	151.4	152.9	427.1	108.5	110.9	112.2	318.6
						Sites (Summer Season)					
Temp.	°C	31.1	32.5	34.6	37	30.4	30.9	30.3	33.1	31.4	31.1
pH	---	7.65	7.71	7.34	7.85	7.63	7.9	7.81	7.62	7.47	7.7
EC	mS/Cm	1.216	0.659	0.671	0.677	0.952	0.775	0.852	0.851	1.296	1.35
TDS	mg/l	750	470	367	271	487	277	273	376	645	778
DO	mg/l	4.7	2.5	5.4	5.11	4.96	3.81	3.65	3.33	2.54	2.77
Turbidity	NTU	10.8	17.2	2.5	10.6	11.1	13.2	6.1	7.2	9.8	12.6
TSS	mg/l	217.2	32.5	40.6	101.1	213.2	76.1	47.2	39.8	192.6	80.8

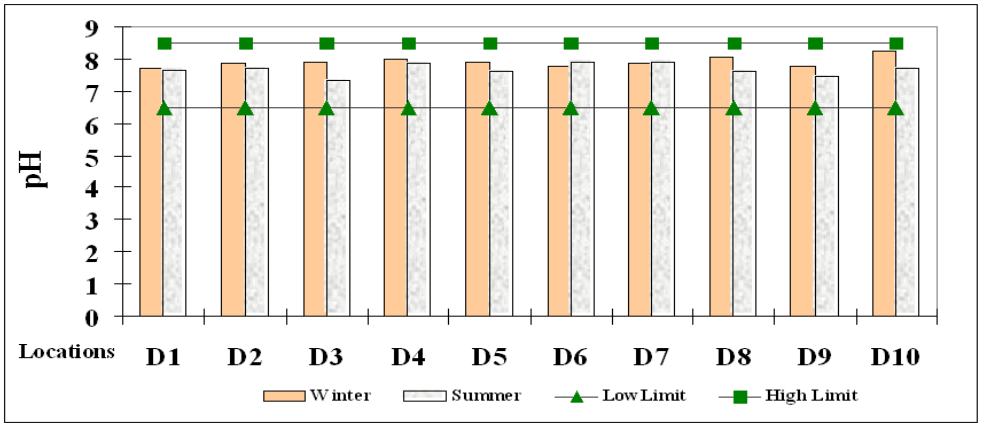

Fig. 7. Seasonal Variations of pH for Drainage Water Samples along El-Moheet Drain

Electrical Conductivity (E.C)

From Table 3, it is seen that E.C values are in the range of 0.748 to 1.85 and 0.659 to 1.35 ms.cm^{-1} during the winter and summer seasons, respectively. Conductance of water samples indicating relatively moderate mineralization and suitable for irrigation purposes in the study area. Fig. 8 showed water undergoes significant fluctuations in E.C. However, EC values are within the permissible limits of FAO, 1985(0.7–3 dS/m**)**.

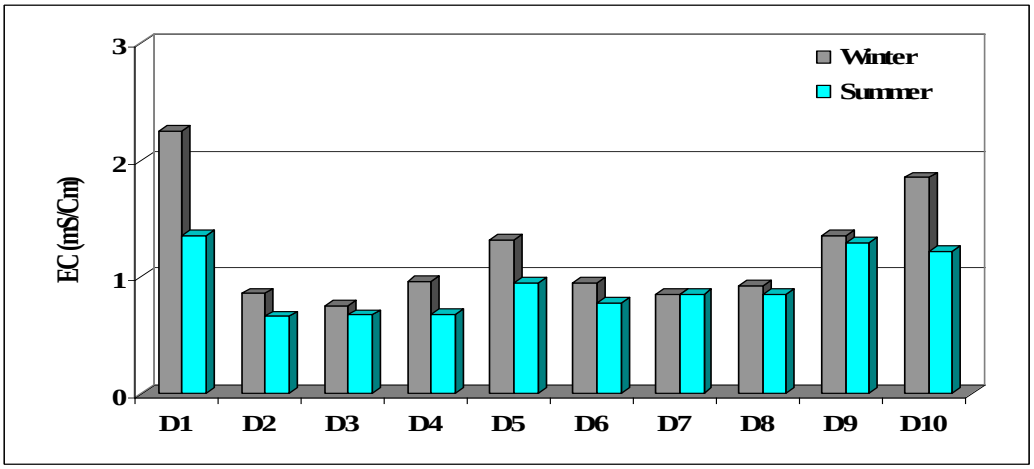

Fig. 8. Seasonal Variations of EC (mS/Cm) for Drainage Water Samples along El-Moheet Drain.

Total Dissolved Solids (TDS)

The estimated values of TDS range from 429 to 975 mg/l and 271 to 778 mg/l during the winter and summer seasons, respectively as in Table 3 and Fig. 9 clarified the results of TDS values of collected drainage water samples are unacceptable desirable limits for all sites in investigated area during winter season except Outlet of Zenien WWTP, Nahia drain and El-Remal drain are below the desirable limits of (Decision 92/2013 of environmental law 48/ 1982).

Dissolved Oxygen (DO)

The study area of DO distribution pattern displays a wide seasonal variation and fluctuated between (1.54 -5.24 mg/l) and (2.5 -5.4 mg/l) during winter and summer seasons, respectively as in Table 3 and Fig. 10 showed the maximum value of DO is observed at SW1during summer. However, the minimum value of DO is recorded during winter at inlet of Zenien WWTP (D2) and El-Rahawy drain (D10). The high concentrations of organic contaminants and nutrients are the main contribution of organic load which consume dissolved oxygen through oxidation processes **(Abinandan et. al., 2014).**

Total Suspended Solids (TSS) and Turbidity

TSS content (turbidity) is considered any suspended matter as organic matter, silt, plankton, clay and other microscopic organisms interfere with the light path thru the water (Fig. 11). FAO, 2017 limits reported <50 mg/l (no restriction on use) and >100 mg/l (Severe restrictions on use for TSS) when irrigating with drip lines **(Peteet et al., 2018)**.

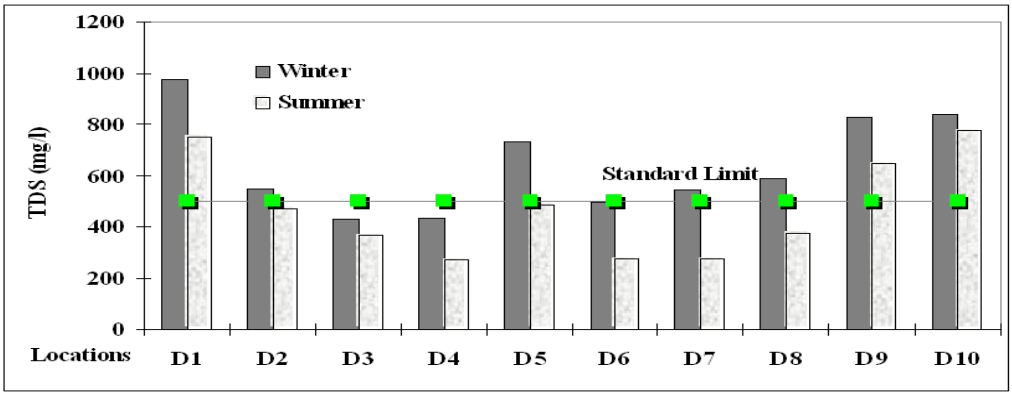

Fig. 9. Seasonal Variations of TDS (mg/l) for Drainage Water Samples along El-Moheet Drain.

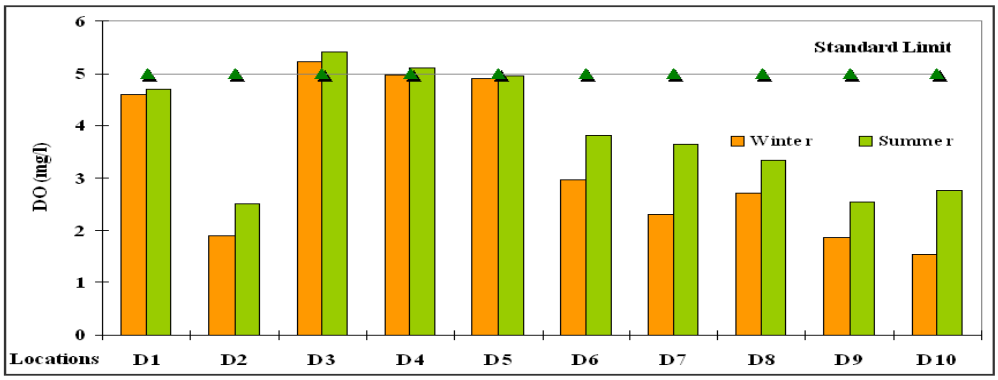

Fig. 10. Seasonal Variations of DO (mg/l) for Drainage Water Samples along El-Moheet Drain.

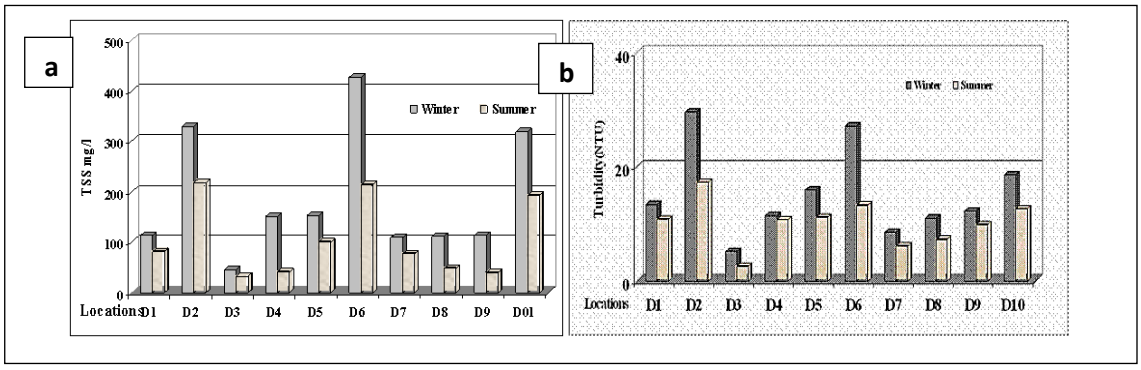

Fig. 11. Seasonal Variations of Turbidity (NTU) and TSS mg/l for Drainage Water Samples along El-Moheet Drain.

On other hand, turbidity describes the degree of particles which water contains, because cloudiness or muddiness resulting in the disturbance of sunlight that turbidity measurement was used as a surrogate **(Peteet et al., 2018)**. Turbidity concentration values in (NTU)

Nephelometric unit for drainage water ranged between (5.1 - 29.6), (2.5 - 17.2) and 45.1 to 427.1, 32.5 to 217.2 mg/l for TSS during winter and summer seasons, respectively. Fig. 11a, b clarified the highest value recorded at inlet of Zenien WWTP (D2), Inlet of Abu-Rawash WWTP (D6) and El-Rahawy drain (D10) during study period that have effect on organisms' life in aquatic environment.

Microbiological Parameters

Total Coliform (T.C) and Fecal Coliform (F.C)

Preliminary survey of biological samples (T.C and F.C) are examined and shown in Table 4 and Fig. 12. All water samples (100%) for both sampling events tested positive for TC bacteria. In general, T.C is higher than F.C for all sources. Some of T.C is most likely the result to benign bacteria that do not reflect sewage contamination **(APHA, 2017 and Noha et al., 2020)**. It is further assumed that the F.C concentration adequately reflects the presence of all microbial pathogens **(Gabriele et al., 2020)**.

The Inlet of Abu-Rawash WWTP (D6), El-Rahwy drain (D10) and Inlet of Zenien WWTP (D2) which exhibit the highest range of T.C and F.C counts during winter and summer seasons, respectively. They represent untreated or partially treated sewage wastes discharged from wastewater treatment plants and effect of sewage on drainage water hence a clear indication of contamination from human wastes. While, high microbial loads record at outlet of D2, D6 and D10 are attributed to the presence of suspended/particulate solids rich in organic matters, which serve as nutrients for the microorganisms **(Samer, 2015)**.

Accordingly, the results of F.C and T.C in some drainage water samples violate the standard limits intended for irrigation according to **(Decision 92/2013 of environmental law 48/ 1982 and FAO, 1985)**.

Table 4. Records of Emergent Organics Concentrations (mg/l) for Water Samples During Winter and Summer Seasons.

Locations	**Winter Season**		**Summer Season**	
	TC	FC	TC	FC
D1	$800X10^3$	$120\ X10^3$	$220\ X10^3$	$100\ X10^3$
D2	$560\ X10^4$	$800\ X10^3$	$133\ X10^4$	$110\ X10^4$
D3	$100\ X10^3$	$20\ X10^3$	$40\ X10^3$	$10\ X10^3$
D4	$140\ X10^3$	$90\ X10^3$	$300\ X10^3$	$170\ X10^3$
D5	$37\ X10^3$	$26\ X10^3$	$120\ X10^3$	$30\ X10^3$
D6	$990\ X10^4$	$400\ X10^3$	$340\ X10^4$	$240\ X10^4$
D7	$70\ X10^3$	$30\ X10^3$	$110\ X10^3$	$74\ X10^3$
D8	$110\ X10^3$	$10\ X10^3$	$620\ X10^3$	$20\ X10^3$
D9	$500\ X10^3$	$250\ X10^3$	$105\ X10^3$	$600\ X10^3$
D10	$400\ X10^4$	$110\ X10^4$	$190\ X10^4$	$90\ X10^3$

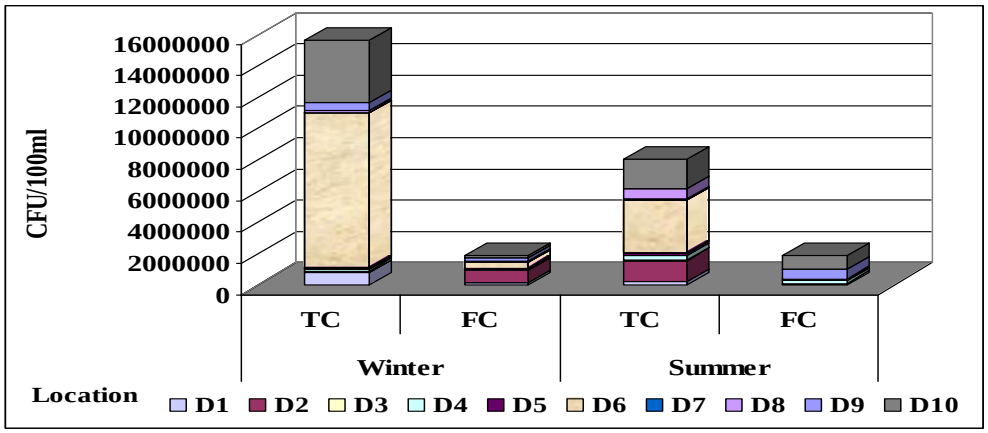

Fig. 12. Seasonal Variations of TC and FC (CFU/100ml) for Drainage Water Samples along El-Moheet Drain.

Quantification of emerging pollutants in water samples
Organophosphorus pesticides

Organophosphorus pesticides (OPPs) have a wide range of industrial and agricultural applications. The studied compounds include (Ethoprop, Terbufos, and Diazinon). Table 5 represents concentration of selected OPPs residues in surface water samples collected from the study area during winter and summer of 2017 -2018. Table 5 showed maximum OPPs concentrations for drainage water samples that recorded 66 ng/l, 62 ng/l and 59 ng/l at El-Rahwy drain (D10), Inlet of Abu-Rawash WWTP (D6) and Inlet of Zenien WWTP (D2) during winter, respectively. This may be due to low flow conditions for water body and lower temperature bringing down the rate of decomposition of organic matter. The high concentrations of organic contaminants and nutrients are the main contribution of organic load **(Alhalafi et al, 2024)**. These values are within the recommended maximum concentrations in irrigation water **(FAO, 1985)** and Decision 92/2013 of environmental law 48/ 1982 limits. Low OPPs values in the summer reflect low burden of organic pollution due to the dilution effect during summer.

Table 5. Records of OPPs residues (ng/l) for Drainage Water Samples DuringWinter and Summer Seasons.

Parameter	D1	D2	D3	D4	D5	D6	D7	D8	D9	D10
					Sites (Winter Season)					
Ethoprop	22	59	15	32	20	62	21	24	<0.01	66
Terbufos	23	44	<0.01	28	28	45	<0.01	<0.01	20	55
Diazinon	<0.01	35	<0.01	22	<0.01	50	18	22	33	58
					Sites (Summer Season)					
Ethoprop	17	33	<0.01	27	<0.01	56	<0.01	18	<0.01	52
Terbufos	11	40	12	26	18	37	14	<0.01	19	39
Diazinon	<0.01	27	<0.01	29	<0.01	33	<0.01	<0.01	22	48

Pharmaceuticals

Pharmaceutical active compounds (PhACs) are a set of developing ecological contaminants that are broadly and progressively being utilized as a part of human and veterinary medication. The detected PhACs in water samples are (paracetamol, Ketoprofen, diclofenac, and ibuprofen). Table 6 represents concentration of selected pharmaceutical residues in surface water samples collected from the study area during winter and summer of 2017 -2018.

Table 6 showed PhACs high values during winter season; that recorded 61 ng/l, 59 ng/l and 57 ng/l this may be due to presence of organic wastes from Inlet of Abu-Rawash WWTP (D6), El-Rahwy drain (D10) and Inlet of Zenien WWTP (D2) during winter, respectively. that clarified during winter there was increasing waste discharge into the drain during low flow condition from the variety of sources (industrial, agricultural, domestic wastes and sewage). In conclusion, variation in levels of PhACs in all drainage water samples can be attributed to geological distribution of minerals that vary from one location to another and anthropogenic activities along El-Moheet drain. that not exceeding permission limits of (Decision 92/2013 of environmental law 48/ 1982). However, the decrease in the PhACs values during summer is mainly attributed to the increase in the water temperatures, facilitating the decomposition and oxidation of organic matter. These results are in agreement with **(Carlos and Isela, 2019 and Ahmed et al., 2022)**.

Table 6. Records of PhACs residues (ng/l) for Drainage Water SamplesDuring Winter and Summer Seasons

Parameter	D1	D2	D3	D4	D5	D6	D7	D8	D9	D10
					Sites (Winter Season)					
Paracetamol	12	55	22	20	13	61	26	24	<0.01	45
Ketoprofen	23	57	16	26	18	55	<0.01	18	23	59
Diclofenac	<0.01	35	<0.01	18	<0.01	43	25	<0.01	33	21
Ibuprofen	09	42	<0.01	23	12	25	32	22	29	32
					Sites (Summer Season)					
Paracetamol	16	47	17	16	<0.01	32	22	18	<0.01	11
Ketoprofen	<0.01	36	11	22	12	26	11	15	19	18
Diclofenac	<0.01	33	<0.01	11	<0.01	22	<0.01	<0.01	27	23
Ibuprofen	07	23	<0.01	15	09	25	18	19	27	25

Removal of Emerging pollutants using banana peels as HCs material

Characterization of prepared materials

The main characteristics of the prepared HCs such as ash content, yield, surface area, average pore diameter, elemental composition and pore volume are exhibited in Table 7. The percentage yields of prepared HCs were found to be fluctuating from 46-86%, and their values reduced gradually with temperature rise from 180-280 °C. At higher temperature (above 180 °C), hemicellulose is preferably hydrolyzed during the hydrothermal carbonization of biomass while cellulose hydrolysis begins around 200-230 °C, which produces high content of sugars as well as organic acids such as acetic, lactic, propenoic, citric, formic acid and others dissolved in liquid phase. Also, lignin degrades at the temperature higher than 200 °C, and the fraction of carbon can exist in liquid and gas phase via decarboxylation and volatilization reactions which are believed to grow with temperature **(Li et al., 2016)**. In contrast to conventional heating methods, the irradiation of microwave is able to activate cellulose molecules, enhance particle collisions and increase hydrolytic efficiency for lignocellulosic biomass under mild conditions and therefore we can find that cellulose hydrolysis occurred at a lower temperature (less than 200 °C) **(Jain et al., 2016)**. These mentioned reasons might be collectively responsible for the decrease in HCs yield at higher hydrothermal temperatures. it can be concluded that the more reaction time, the less HCs yield which could be ascribed to the stubborn decomposition of the structural components of banana peels in a hydrothermal environment. In addition, the ash content for all samples is very low which less than 1.23%. This could be attributed to dissolution and elimination of inorganic minerals from the HCs surfaces as water molecules act as a solvent along with a reactant during the hydrothermal process **(Li et al., 2019)**. Due to their low ash

contents, the prepared HCs could be auspicious adsorbents during wastewater treatment without causing secondary pollution.

Table 7. Outline the characterization of HC;ash content, yield, surface area, average pore diameter, elemental composition and pore volume.

Sample	Temp. °C	Reaction time (h)	Yield %	Ash content %	Surface area (m^2/g)	Pore volume (cm^3/g)	Average pore diameter (nm)	C (%)	H (%)	N (%)	S (%)
I-1	180	0.5	76.4	0.46	152.02	0.23	3.51	44.2	5.5	0.28	0.06
I-2	180	1	86.2	0.33	188.69	0.25	3.42	44.6	5.1	0.26	0.06
I-3	180	3	72.6	0.68	121.69	0.19	3.47	45.8	5.2	0.27	0.14
II-1	210	0.5	73.3	0.85	178.21	0.26	3.38	47.6	4.8	0.32	0.17
II-2	210	1	68.5	0.44	162.07	0.24	3.65	48.9	4.8	0.3	0.15
II-3	210	3	62.3	0.35	115.87	0.17	3.61	49.8	4.6	0.35	0.14
III-1	250	0.5	53.6	0.45	166.25	0.26	3.41	54.5	4.3	0.46	0.09
III-2	250	1	49.8	0.71	152.21	0.22	3.08	56.4	4.3	0.48	0.10
III-3	250	3	47.3	0.62	109.92	0.15	3.24	59.4	3.7	0.55	0.06
IV-1	280	0.5	48.2	0.74	168.25	0.28	3.18	62.1	3.6	0.61	0.12
IV-2	280	1	49.8	1.23	175.32	0.32	3.25	63.1	3.7	0.65	0.12
IV-3	280	3	46.1	0.82	102.32	0.12	3.32	65.2	3.4	0.68	0.12

FTIR for Hydrochar(HC)and HCnanoparticles

The FTIR spectra (Fig. 13) of HC and HC-TiNPs showed that the hydrochar prepared in our study is rich in several functional groups on the surfaces, principally O-containing functional groups, and these groups could promote chemical or partially-chemical adsorption instead of purely physical adsorption for organics on the hydrochar. As noticed, the modification of hydrochar did not change the surface functionality and thus would keep the adsorption performance. The strong and broad peak observed in section (3600-3000 cm^{-1}) is due to the aliphatic OH stretching vibration of hydroxyl and carboxyl functional groups. While the peaks in section (3000-2800 cm^{-1}) are due to the C-H stretching vibration. Additionally, the peaks in section (1800-1600 cm^{-1}) corresponds to the stretching vibration of C=O bonds in carboxylic acids, esters, or aldehydes from cellulose. While the peak in Section 4 (1600-1500 cm^{-1}) corresponds to the C=C vibrations of the aromatic rings in lignin. After the hydrothermal carbonization process, this peak reduced indicating that the lignin only decomposed partially under the studied condition, while those in Section 5 (1450- 1200 cm^{-1}) corresponds to the C-H bending vibration of aliphatic carbons, methylene, and methyl groups, which shows that aliphatic structures are present. Whereas the peaks between 1000 cm^{-1} and

1200 cm^{-1} represent C–O bending vibrations from esters, phenols, and aliphatic alcohols. The peaks appeared below 1000 cm^{-1} results from the distortion of the C–H bonds in aromatic compounds **(Tejada-Tovar et al., 2019)**.These obtained results are agreed with the oxygen and carbon contents of the HC samples (Table 6), which could be due to the polymerization and condensation reactions in HTC and reproduce a surface with excessive active sites**.** From Fig. 13**,** we can say that the microwave method protects the function groups through hydrochar production as agreed with **(Parshetti et al., 2014)**. Table 8 presents the Function groups that appeared in banana peels feedstock and its hydrochar.

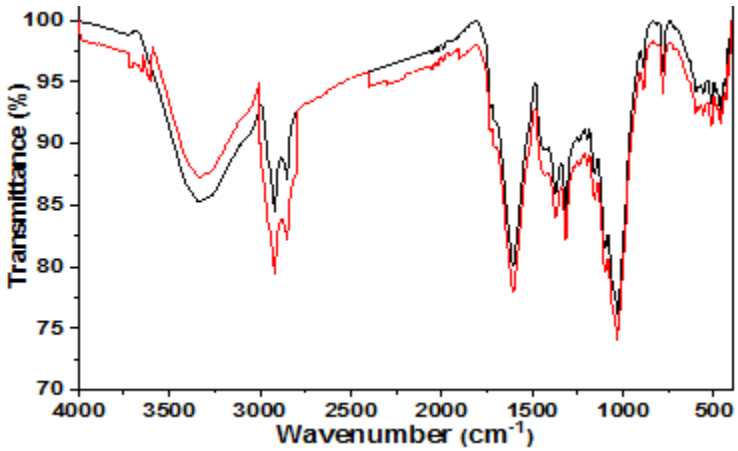

Fig.13. FTIR spectra of HC (Redline) and HC-TiNPs (Black line).

Table 8. Function groups appeared for banana peels feedstock and its hydrochar.

Range cm^{-1}	< 1000	1000-1200	1200-1450	1500-1600	1600-1800	2800-3000	3000-3600
BP	O-H	aromatic = C-H	C-O	C=C	C=O	al C-H	R-COOH, OH
HC	O-H		C-O		C=O	al C-H	R-COOH, OH

SEM- EDX

The hemicellulose is destroyed during the degradation and depolymerization reactions due to thermal pretreatment of biomass, which leads to the loss of structure. The destroyed structure has increased friability **(Bashir et al., 2021)**. The heterogeneous structure of HC was investigated by SEM as shown in Fig. 14. It can be notice that the HC surface has groove-like orientations with dense morphology. Also, there is unequal distribution of pores on the surface of the hydrochar sample, and the pore structures are clearly unlimited. Additional

adsorption sites are provided due to the rough surface and pore structure of hydrochar. EDX elements mapping results as provided in Fig. 15 proved the presence of titanium which relates to TiNPs on the HCs surface.

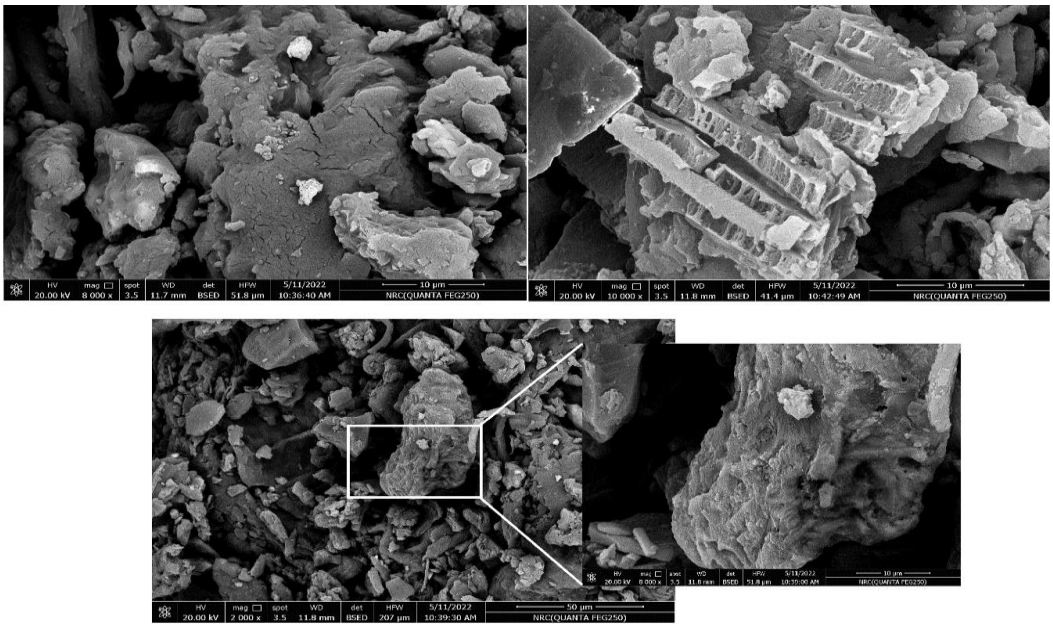

Fig. 14. SEM images of prepared hydrochar.

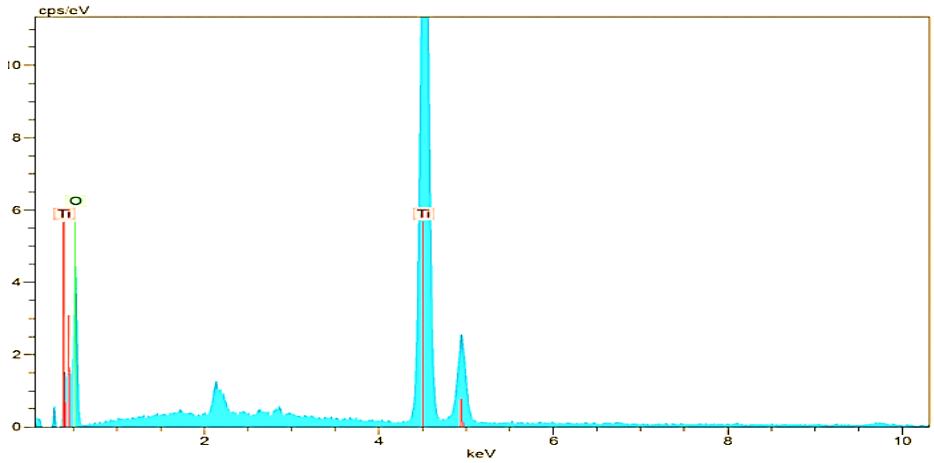

Fig. 15. The EDX analysis of modified hydrochar with TiNPs**.**

XRD for HC -TiNPs

XRD patterns of HC-TiNPs were presented in Fig. 16. As seen from the curve, two peaks obtained at 2θ = 14.7° and 24.2°, which correspond to the crystal planes of (101) and (002) respectively, representing the presence of graphitic aromatic ring structures **(Rizk et al., 2017)**. Besides, the peaks appeared at 2θ = 28.1°, 38°, 40.2° and 50.2° could be assigned to

the crystal face structures of TiO_2 indexed planes (i.e., (220), (311), (400) and (422)), indicating the existence of TiO_2 on the HCs surface **(Bashir et al., 2021)**.

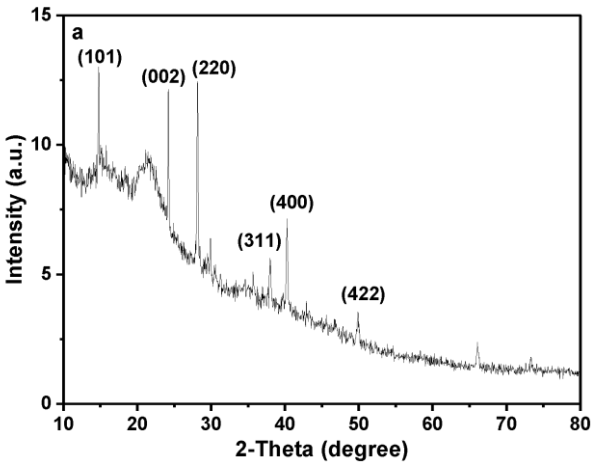

Fig. 16. XRD patterns of HC-FeNPs.

BET surface area

The BET surface areas, pore volumes and average pore diameters of the banana peels hydrochar estimated from the N_2 adsorption–desorption isotherms are recorded in Table 7. The BET specific surface areas of the hydrochar adsorbents were measured to be from 75.32 m^2/g to 188.69 m^2/g, the pore volumes were between 0.07 cm^3/g and 0.32 cm^3/g, and the average pore diameters were determined in the range from 3.08 nm to 3.65 nm. The banana peels hydrochars reported in this study have higher BET specific surface areas and pore volumes than those of some prepared hydrochars in previous studies **(Elaigwu and Greenway, 2016)**. As shown in Table 7, it was noticed that the more reaction time, the higher surface areas as well as the pore volumes of the prepared hydrochars when the reaction time is set to be 0.5 and 1 h, whereas a negative effect was observed in case of longer reaction time (3 h). The biomass hydrothermal carbonization process undergoes a multistep reaction mechanism starting from biomass hydrolysis which produce low-molecular weight molecules such as amino acids, oligosaccharides and glucose (or fructose), and this step could has positive impact on pore forming to secure higher surface areas and pore volumes for hydrochars **(Jain et al., 2016)**. By the time, the carbonization stage begins and the hydrolyzed glucose (or fructose) are dehydrated to 5- hydroxymethylfurfural (HMF). The hydrochar is produced from both HMF polymerization and the conversion of solid biomass via intramolecular condensation, devolatilization and decarboxylation. These mechanisms generally require a much higher temperature (over 200 °C), and they have a negative effect on forming and expanding pores, which may result in the complex impact of the hydrothermal carbonization temperature on the pore properties of the produced hydrochars **(Ameen et al.,**

2022). Fig. 17 shows nitrogen adsorption/desorption isotherms of HC-TiNPs composite and its corresponding pore size distribution curves.

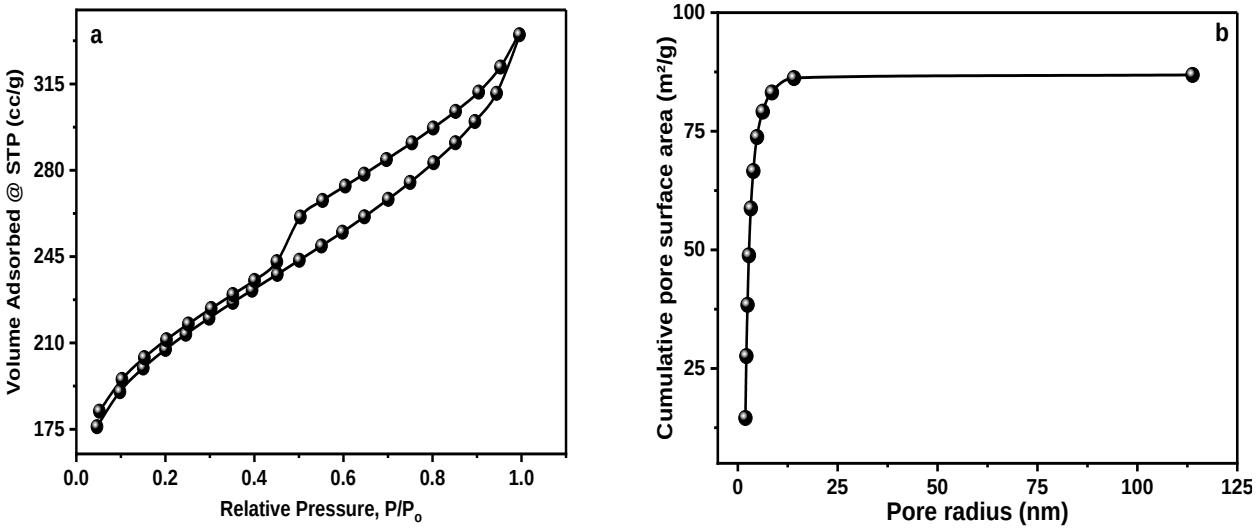

Fig. 17. (a) N_2Adesorption/desorption isotherms of HC-FeNPs (b) its corresponding pore size distribution curve.

The mechanism of the HC process

Principally entails complex reaction network including decarboxylation, dehydration, and polymerization (aromatization). Removing carboxyl and single bond OH groups decrease the O/C ratio meaningfully produce the final product. According to the elemental analysis (Table 7), the carbon content of the prepared HCs increases with higher hydrothermal carbonization temperature and more reaction time, but hydrogen and oxygen contents decreased. This confirms dehydration and decarboxylation reactions during carbonization process, and the more aromatization in produced HCs at higher hydrothermal temperatures and reaction time. These findings agree with former literatures **(Li et al., 2016)**. What's more, both hydrolysis and polymerization steps can be accelerated by microwave ultrasonic in hydrothermal carbonization process, which means higher content of carbon in the final product **(Mahmoud et al., 2024)**. Additionally, the high oxygen content (30.46%-49.85%) demonstrating rich oxygen-containing groups on produced HCs surfaces whereas the low contents of both nitrogen (<0.7%) and sulfur (<0.2%) make the prepared HCs beneficial adsorbents without causing secondary pollution in the environment.

Adsorption studies for organophosphorus pesticides (OPPs)

Fig. 18a displays the adsorption performance at initial concentration of 1 mg/mL and 25 °C for the three insecticides on the banana peels hydrochars. Generally, the hydrochars

prepared in this study are able to eliminate all the three pollutants with more than 80% efficiency. The hydrochars exhibit slightly dissimilar elemental compositions and surface functional groups, most of them show comparable BET surface areas and pore volumes, and the complex effects of these might be responsible for their close and apparently random adsorption capabilities for pollutants. Sample I-2 was selected for studying the adsorption. Sample I-2 providing higher adsorption amounts for the adsorbates and having higher yields among other hydrochar samples was selected to be modified with TiNPs for the subsequent tests. The modification of hydrochar with TiNPs had nearly no effect on the adsorption performance (Fig. 18), however, the modified hydrochar has magnetic property and therefore could be easily recovered from the solution.

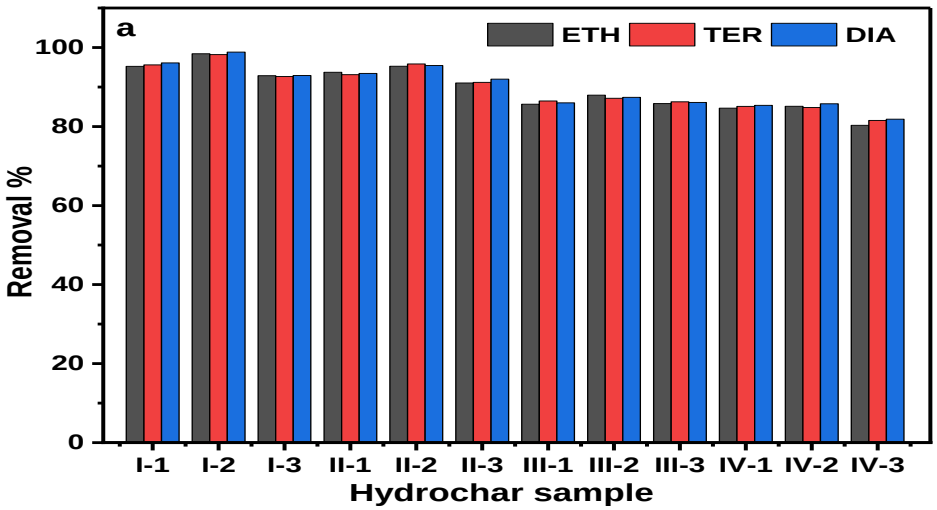

Fig. 18. Adsorption performance of three insecticides on prepared the banana peels hydrocharssamples (I-1 to IV-1) and modified with TiNPs[(I-2 to IV-2) and (I-3 to IV-3)] at concentration of 1.5 mg/mL and 1 mg/mL respectively in 25 °C.

Dosage effect on adsorption capacities

The adsorbent dosage effect of HC-TiNPs was studied by varying the adsorbent quantity from 40-90 mg keeping the contact time; 3 h, initial concentration of three insecticides; 1.5 (mg/L), at 25 °C. Fig. 19 represents the effect of adsorbent dosage on OPPs removal efficiency. As noticed, the removal efficiency exceeded 95% for all three compounds, illustrating that HC-TiNPs would be a promising and effective adsorbent for OPPs removal. Taking the characteristics of HC-TiNPsinto account, the plentiful functional groups and the porous surface structure are responsible for the high adsorption performance. In addition, the removal % improved by increasing the adsorbents amount till 70 mg of adsorbent, then the change was not remarkable after further increase. This phenomenon is normal because adding more amount of adsorbent material means an increased in the number of adsorption active sites in the medium and hence, improved adsorption performance. The effective adsorbent dosage selected for the subsequent experiments was 70 mg.

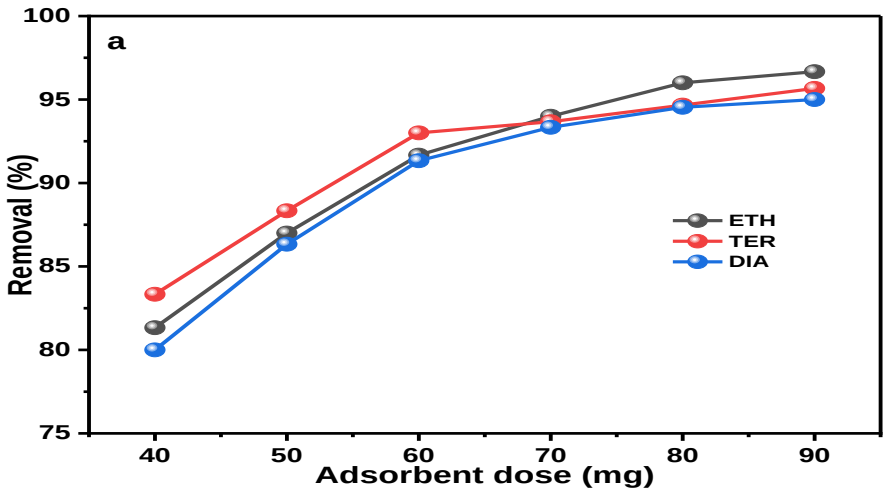

Fig. 19. Effect of amount of adsorbent on the removal efficiency of ETH, TER and DIA.

Contact time effect

The adsorption efficacy is based on the equilibrium of the interaction between the adsorbent active sites and insecticides molecules. The effect of contact time on the simultaneous adsorption of ETH, TER and DIA by HC-TiNPs was examined with time profile for 20-240 min with keeping adsorbent dosage; 70 mg, pH; 4, initial concentration of three insecticides; 1.5 (mg/L), at 25 °C and the data are presented in Fig. 20. At the beginning, the adsorption rate of pollutants was rapid and then reached its equilibria after 3 h, with extraction rates higher than 93% for the three studied insecticides. This can be explained by the fact that the binding sites were unoccupied on initial stages, which were then occupied by pollutant molecules. This means the 3 h is enough time for organophosphorus pesticides removal from the solution and this interval is selected for further experiments.

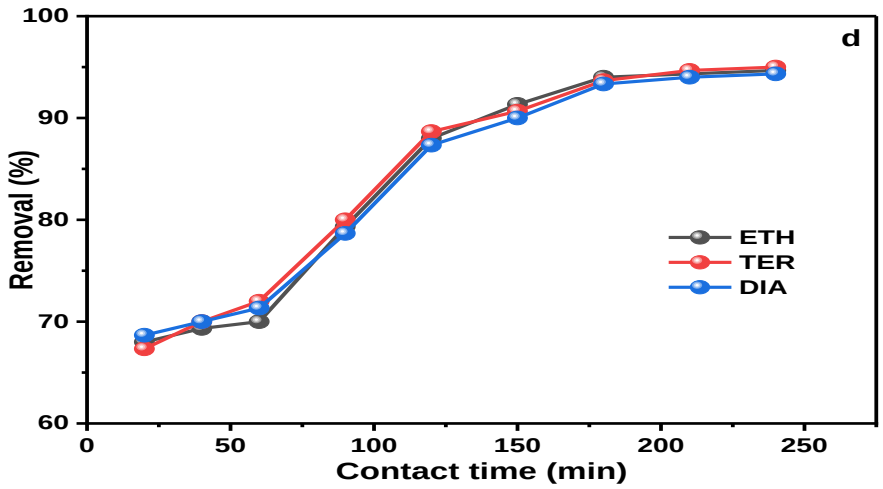

Fig. 20. Effect of contact time on the removal efficiency of ETH, TER and DIA.

Adsorption kinetics

The study of adsorption kinetics is very valuable for better understanding of insecticides adsorption mechanism adsorption process in terms of the order and the rate constant which is important for designing an efficient adsorption operation. The most well-known adsorption kinetic models have been used in the literature to explain the adsorption mechanism. The derived rate constants together with the correlation coefficient R^2 for the three studied insecticides are illustrated in Table 8 and the best-fitting plots are shown in Fig. 21 (a-d). The goodness of fit of either kinetic model is identified by the value of the correlation coefficient (R^2) closer to unity. Also, the good agreement of calculated adsorption capacity (calculated q_e) and the experimental values (experimental q_e) is another significant criterion **(Zhu et al., 2015)**. Consequently, the lower values of R^2 and the variance between experimental and calculated equilibrium demonstrates that the kinetic model failed to express the adsorption kinetics.

Pseudo-First-order kinetic for OPPs removal

For the pseudo 1st order kinetic model, the correlation coefficients were found to be moderately low ($R^2 \leq 0.89$) as well as the difference between calculated and experimental adsorbed amounts at equilibrium is relatively high, which demonstrated a bad fit between the experimental data and the model. So, the adsorption of organophosphorus insecticides onto HC-TiNPs is not an ideal pseudo 1st order reaction.

Pseudo-Second-order kinetic for OPPs removal

The pseudo 2nd order kinetics model exhibited the excellent regression coefficients (R^2> 0.99 for all three insecticides). Furthermore, it showed the adsorption capacity of 2.18, 2.16 and 2.15 mg/g, which were adequately close to the amount of the experimental adsorption capacity 2.01, 2.00, and 2 mg/g for ETH, TER and DIA, respectively. As a consequence, the adsorption process is an ideal pseudo 2nd order reaction. These results indicate that the chemisorption could be the rate-determining step in the adsorption of the organophosphorus insecticides determining step in the adsorption of the organophosphorus insecticides.

Intraparticle diffusion kinetic for OPPs removal

Although the experimental data are in a good accordance with the pseudo 2nd order model, this model is not able to define the adsorption mechanism. Therefore, intraparticle diffusion kinetic model was applied to combat this limitation. If intraparticle diffusion contributes to the adsorption reaction, a linear relationship between $q_t$vs t½ would be obtained and if the line passed through the origin, then it is the rate-limiting step. In general, in the solid-liquid adsorption, the movement of adsorbates molecules is normally described by external diffusion (also known as film diffusion), surface diffusion, pore diffusion, or mutual

surface and pore diffusion (Kebede et al., 2020). In the first stage (within 60 min), the adsorbate molecules diffused to the adsorbent external surface is the external surface adsorption and this stage is the external surface adsorption. The second stage (from 60 to 180 min) was the gradual adsorption phase, where intraparticle diffusion was the rate-controlling step. The third portion is the equilibrium stage, which is the final phase where intraparticle diffusion began to decelerate because of the extremely low concentrations of adsorbate molecules in the solution and/or the inadequate number of available active sites (Zhu et al., 2015). In addition, it is observed the straight lines did not go through the origin, implying that some degree of boundary layer has impact on the adsorption process which means that the intraparticle diffusion is not the only rate-controlled mechanism and the adsorption rate may be controlled by other kinetic models might control, all of which could be operating concurrently.

Table 8. Kinetic parameters for organophosphorus insecticides adsorption by HC-TiNPs.

Kinetic model	**ETH**	**TER**	**DIA**
Experimental q_e (mg/g)	2.01428	2.0071	2
Pseudo-first order model			
q_e Calculated (mg/g)	3.23571	2.97130	4.93409
k_1	-0.00014	-0.00014	-0.00017
R^2	0.886	0.896	0.854
Pseudo-second order model			
q_e Calculated (mg/g)	2.18708	2.16962	2.15786
k_2	0.02383	0.02581	0.02568
R^2	0.994	0.996	0.995
Intra-particle diffusion model			
K_{dif} (mg/g^{-1} min$^{-0.5}$)	1.12428	1.14575	1.15936
C (mg/g)	0.06248	0.06088	0.05869
R^2	0.916	0.934	0.928
Elovich model			
α (mg/g min)	2.24427	2.18932	2.19485
β (g/mg)	0.31213	0.29635	0.29044
R^2	0.880	0.917	0.888

Elovich kinetic for OPPs removal

Elovich equation was useful in description of systems where the surface of the adsorbent is highly heterogeneous and also it shows that accompanied by surface adsorption chemisorption is also a dominant phenomenon taking place **(Riahi et al., 2017)**. The values of α and β were calculated from the plot of q_t vs. ln t (Fig. 21d). The corresponding constant values are presented in Table 8. The values given in Table 2 reveal that the correlation coefficients are lower than those of the pseudo 2nd order model and the Elovich kinetic model

equation do not provided a very good fit to the adsorption kinetic data based on the low values of the R^2. The Elovich equation does not predict any certain mechanism. In general, Table 8 reveals that pseudo 2nd order and intraparticle diffusion kinetic models adequately fit the organophosphorus insecticides-hydrochar adsorption data, and accordingly supports the assumption behind the model that the adsorption of insecticides onto hydrochar is due to chemisorption.

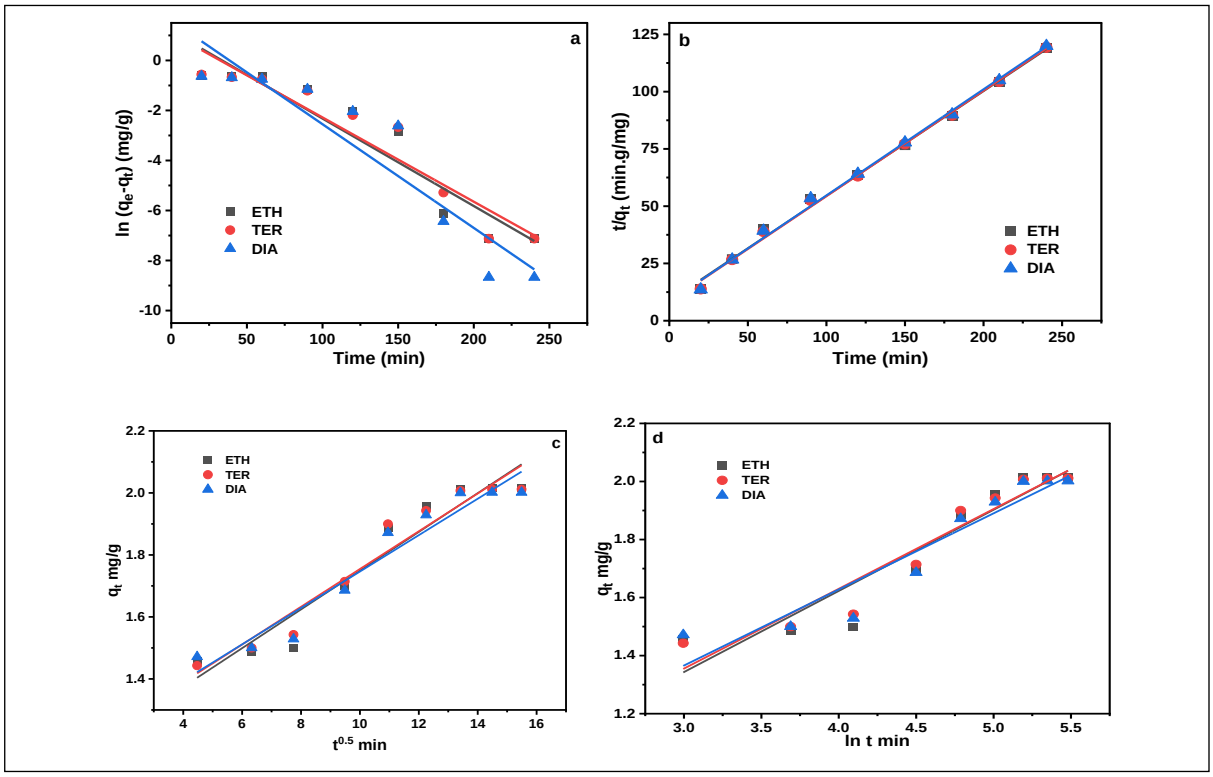

Fig. 21a-d. (a). Pseudo-first order kinetics for adsorption of OPPs, (b).Pseudo-second order kinetics for adsorption of OPPs (c).Intraparticle diffusion kinetics for adsorption of OPPs, (d). Elovich kinetics for adsorption of OPPs on HC-TiNPs

Adsorption isotherms

Adsorption isotherms are significant to explain how an adsorbent can interact with adsorbate molecules and scrutinize the adsorption mechanism, hence assist in improving the design of a specific adsorption process. In the current study, the equilibrium data obtained for removal of organophosphorus insecticides using HC-TiNPs was tested with four isotherm models (Freundlich, Langmuir, Temkin and D-R isotherms) presented in the literature to disclose the best fitting isotherm **(Zelmanov et al, 2008)**. Table 9 the model parameters of four isotherms for the elimination of three organophosphorus insecticides using HC-TiNPs.

Figs. 22a-5d demonstrates the experimental data points and the fitted lines for different initial concentrations of studied insecticides.

Isotherm of OPPs adsorption using Freundlich model for heterogeneous surface energy systems and for the description of multilayer adsorption with the interaction between adsorbed molecules. The Freundlich isotherm can be defined by Equation (8). The plot for lnqe against lnCeFig. 22a.Showed the multilayer coverage of pollutants at HC-TiNP surface. The obtained results showed Freundlich isotherm (($R^2 \leq 0.90$).

Isotherm of OPPs adsorption using Langmuir model

Adsorption data are commonly characterized by the equilibrium isotherm value, which is a plot of the Ce/qe as a function of Ce according to the Langmuir model as shown in Fig 5b. The raw data for the Langmuir model is provided in Table 3 The obtained results showed Langmuir isotherm ($R^2 \geq 0.99$).

According to the results illustrated in Table 9, the correlation coefficients values indicated that the Langmuir model ($R^2 \geq 0.99$) can fit the adsorption isotherm data well for all the three pollutants compared to the Freundlich model (($R^2 \leq 0.83$). Thus, the equilibrium adsorption data can be described more precisely by the Langmuir isotherm than the other isotherm models. Based on the Langmuir theory, it can be concluded that the adsorption of ETH, TER and DIA on HC-TiNPs is monolayer, and the surface of HC-TiNPs is homogeneous without significant lateral interactions between the insecticides molecules. Normally, carbonaceous materials are good adsorbents of microwave, and in contrast to the conventional heating approaches, microwave irradiation offers the merits of heating the material from the interior body, uniform heating and so forth (Li et al., 2019).

It can be deduced that these could result in producing hydrochar with homogenous surface and thus responsible for the good fitting of Langmuir equation to the adsorption isotherms. The obtained maximum adsorption capacity (q_{max}) values of HC-TiNPs using Langmuir isotherm model were 3.19, 3.07 and 3.19 mg/g for ETH, TER and DIA, respectively. The 1/n values from Freundlich model were calculated to be 0.398 for ETH, 0.407 for TER and 0.406 for DIA, less than 1, implying that the adsorption is a favorable process for all studied organophosphorus insecticides on the HC-TiNPs.

Isotherm of OPPs adsorption usingTemkin model

According to the Temkin isotherm, the adsorption heat of all phase molecules decreases linearly as the adsorbent is saturated and there is a fixed uniform bond energy distribution. The adsorption data were evaluated according to the linear form of the Temkin isotherm Eq. (12) and according to the results presented in Table 3, the values of K_T and B_T showed a good variation in heat of adsorption and good interactions between insecticides molecules and HC-TiNPs. Temkin model shown in Fig 22c.

Table 9. Comparison of the coefficients isotherm parameters for organophosphorus insecticides adsorption onto HC-TiNPs.

Adsorption model	**ETH**	**TER**	**DIA**
Freundlich isotherm			
1/n	0.3982	0.40769	0.40623
K_f	3.32452	3.64124	3.39179
R^2	0.828	0.819	0.828
Langmuir isotherm			
q_{max} *(mg/g)*	3.19948	3.07083	3.19233
K_L	12.2906	8.69249	11.9927
R_L	0.05145	0.07123	0.05266
R^2	0.992	0.980	0.993
Temkin isotherm			
K_T *(L/mol)*	231.397	199.223	215.369
B_T *(kJ/mol)*	0.51349	0.56384	0.52737
R^2	0.937	0.960	0.943
D-R isotherm			
q_{max} *(mg/g)*	2.95287	3.05934	2.97415
B (mol^2/kJ^2)	1.59E-08	1.63E-08	1.60E-08
E (kJ/mole)	5614.57	5547.00	5598.20
R^2	0.978	0.978	0.980

Isotherm of OPPs adsorption using D-R model

On the other hand, D-R model is a semiempirical equation which is applied to evaluate the characteristic porosity and the apparent free energy of sorption. The calculated values of E are reported in Table 9. The obtained q_{max} values using D-R isotherm model for adsorption of ETH, TER and DIA over HC-FeNPs were 2.95, 3.05 and 2.97, respectively, which are so close to those reported from the Langmuir isotherm model. Also, the R^2 values obtained from the D-R equation in respect to the three compounds were higher than 0.97, indicating that the adsorption of organophosphorus insecticides obeys the D-R equation. D-R model shown in Fig 22d

Conclusion

The liquid agricultural and industrial wastes poured adjacent to El-Moheet drain have negative impacts on the aquatic environment and harmful society. These studies motivated on some emerging pollutants in the agricultural wastewater as pesticide and pharmaceuticals residues. Moreover, the study exhibits the advanced treatment technologies used in wastewater treatment to quality and reuse it. A talented HC-TiNPs was prepared from hydrochar banana peels and TiNPs via a hydrothermal microwave-ultrasonic assisted carbonization technique. The HC-TiNPs was characterized with BET surface area, FTIR, and

good stability bio adsorbent. Furthermore, the composite assessed for removal of highly toxic organophosphorus insecticides and Pharmaceuticals from aqueous solutions. The optimized structures from DFT study are indicated strong adsorption due to negative charge transfer from MOF to the insecticide. Four important operating parameters containing adsorbent dosage, initial concentration of insecticides, pH and incubation time were optimized and found to be 1229 mg, 681 mg/L, for 3h for insecticides and 982 8 mg/L for 4h for Pharmaceuticals respectively. The kinetic sorption data revealed both of the insecticides and pharmaceuticals adsorption was administered by 2nd order mutually with intraparticle diffusion kinetic model. The adsorption isotherms of three insecticides and four pharmaceuticals studied onto HC-TiNPscan agree well with Langmuir adsorption model.

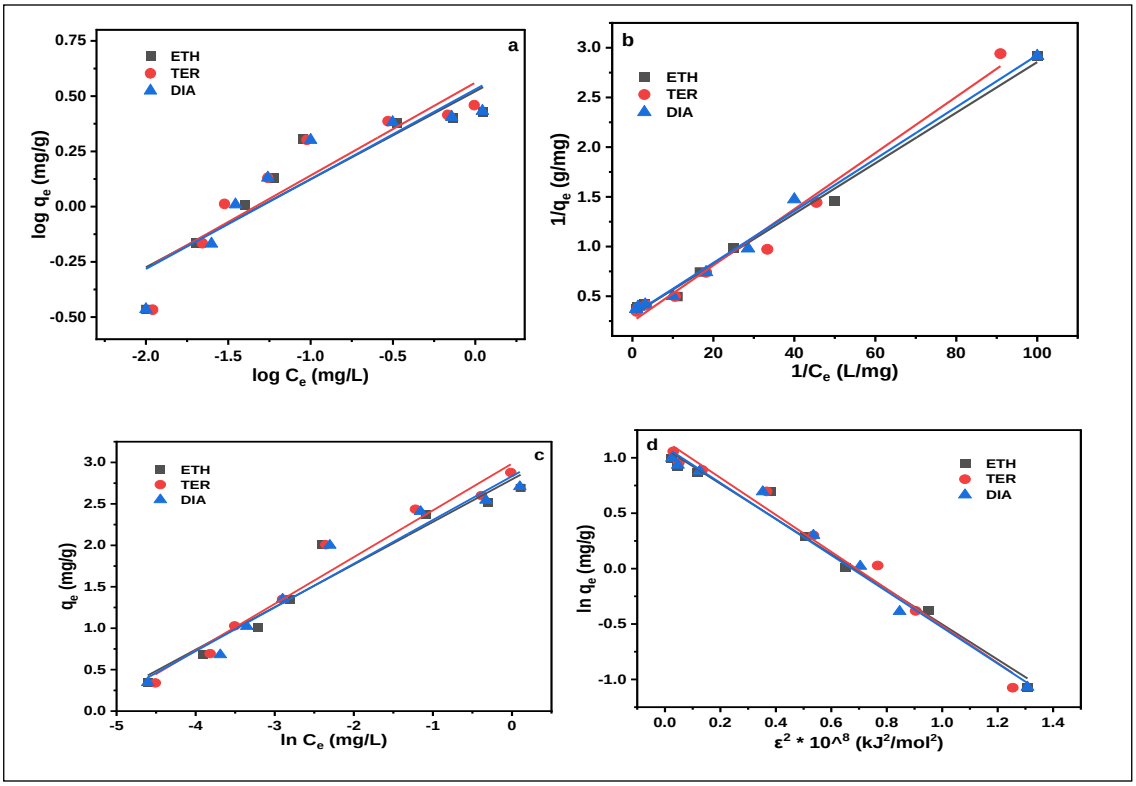

Fig. 22a-d. (a). The linear fitting curve of Freundlich isotherm model for adsorption of OPPs. (b). The linear fitting curve of Langmuir isotherm model for adsorption of OPPs. (c). The linear fitting curve of Temkin isotherm model for adsorption of OPPs. (d). The linear fitting curve of D-R isotherm model for adsorption of OPPs on HC-TiNPs.

References

Abinandan, S., Anand, B.A., Subramaniam, S. 2014. Assessment of physicochemical characteristics of groundwater: A case study. Int. J. Environ. Health Eng.,3, 6. https://doi.org/10.4103/2277-9183.131809.

Alhalafi, M.H., Rizk, S.A., Al-Malki, E.S., Algohary, A.M. 2024. Microwave- ultrasonic assisted extraction of lignin to synthesize new nano micellar organometallic surfactants for refining oily wastewater. *Bioresources and Bioprocessing*, 11(1), 46

Alotaibi, B., Rizk, S.A., Alyousef, H.A., Atta, A., Elgendy, A.T. 2024. Green synthesis of aryl-(4-oxo-1,2-dihydroquinazolin-4-yl-methylene) pyrazole-TiO2 nanoparticles as dyes removable for waste water treatment Applied Organometallic Chemistry, 38(1), e7307

Alotaibi, B.M., Alyousef, H.A., Atta, A., Rizk, S.A., Elgendy, A.T. 2024. Influence of TiO2 Nanoparticles on Enhancing the Properties Activity of Organic Polymeric Materials for Industrial Applications. *ECS Journal of Solid State Science and Technology*, 13(6), 063005

Dutta, A.K., Maji, S.K., Adhikary, B.2014. C-Fe_2O_3 nanoparticles: an easily recoverable effective photo-catalyst for the degradation of rose bengal and methylene blue dyes in the waste-water treatment plant. Mater. Res. Bull. 49, 28–34.

El Saliby, I.J., Shon, H., Kandasamy, J., Vigneswaran, S. 2008. Nanotechnology for wastewater treatment: in brief. Encyclopedia of Life Support Syst. (EOLSS).

Elsayed, H., Djordjevic, S., Savic, D., Tsoukalas, I., Makropoulos, C. 2022. Water-food-energy nexus for transboundary cooperation in Eastern Africa. Water Supply, 22, 3567–3587. https://doi.org/10.2166/WS.2022.001

Gupta, V.K., Tyagi, I., Sadegh, H., Shahryari-Ghoshekand, R., Makhlouf, A.S.H., Maazinejad, B. 2015. Nanoparticles as adsorbent; a positive approach for removal of noxious metal ions: a review. Sci. Technol. Dev., 34, 195.

Hamza, M.A., Rizk, S.A., Ezz-Elregal, E.-E.M., Ramadan, S.K., Abou Gamra, Z.M. 2023. Photosensitization of TiO2 microspheres by novel Quinazoline-derivative as visible-light-harvesting antenna for enhanced Rhodamine B photodegradation Scientific Reports, 13(1), 12929 https://doi.org/10.1038/s41598-023-38497-9

Hamza, M.A., Abd El-Rahman, S.A., Ramadan, S.K., Rizk, S.A., Abou-Gamra, Z.M. 2024. Theenhanced visible-light-driven photocatalytic performance of nanocrystalline TiO_2 decorated by quinazolinone-photosensitizer toward photocatalytic treatment of simulated wastewater. *Journal of Photochemistry and Photobiology A: Chemistry*, 452, 115599.https://doi.org/10.1002/aoc.7307

Kalfa, O.M., Yalc¸ınkaya, O., Turker, A.R. 2009. Synthesis of nano B_2O_3/TiO_2 composite material as a new solid phase extractor and its application to preconcentration and separation of cadmium. J. Hazard. Mater. 166, 455–461.

Khajeh, M., Sanchooli, E. 2011. Synthesis and evaluation of silver nanoparticles material for solid phase extraction of cobalt from water samples. Appl. Nanosci., 1, 205–209.

Khajeh, M., Silver nanoparticles for the adsorption of manganese from biological samples. Biol. Trace Element Res. 2010, 138, 337–345.

Kyzas, G.Z., Matis, K.A. 2015. Nanoadsorbents for pollutants removal: a review. J. Mol. Liq., 203, 159–168.

Mahmoud, H.N.S., El-Shazly, M.A.M., Saad, A.M., Ghareeb, M.A., Rizk, S.UPLC. 2023. QTOF/MS-assisted chemical profiling of Daucus carota leaf extract and evaluation of its antioxidant, antimicrobial and antibiofilm activities: Evidence from in vitro and in silico studies. *Egyptian Journal of Chemistry*, 66(13), pp. 2175–2190

Mohamed, Y.A., Rashad, M. 2012. Water resources management: case study of Sharkia governorate, Egypt. Appl. Water Sci., 22 2, 95–99. https://doi.org/10.1007/S13201-012-0026-5

Nassar, A.E., El-Aswar, E.I., Rizk, S.A., Gaber, S.E.-S., Jahin, H.S. 2023. Microwave-assisted hydrothermal preparation of magnetic hydrochar for the removal of organophosphorus insecticides from aqueous solutions. Separation and Purification Technology, 306, 122569 https://doi.org/10.1016/j.seppur.2022.122569

OECD (Organisation for Economic Co-operation and Development), 2010. List of Manufactured Nanomaterials and List of Endpoints for Phase One of the Sponsorship Programme for the Testing of Manufactured Nanomaterials: Revision; Series on the Safety of Manufactured Nanomaterials Organisation for Economic Cooperation and Development, Paris, 27.

Palamuleni, L., Akoth, M. 2015. Physico-Chemical and Microbial Analysis of Selected Borehole Water in Mahikeng, South Africa. Int. J. Environ. Res. Public Heal. 12, 8619-8630. https://doi.org/10.3390/IJERPH120808619

Peteet, D.M., J. Nichols, T. Kenna, C. Chang, J. Browne, M. Reza, S. Kovari, L. Liberman, and S. Stern-Protz, 2018: Sediment starvation destroys New York City marshes' resistance to sea level rise. *Proc. Natl. Acad. Sci.*, 115, no. 41, 10281-10286, doi:10.1073/pnas.1715392115.

Rizk, S.A., Alzahrani, A.Y., Abdo, A.M. 2024. Enantioselective MW-US-assisted Synthesis, DFT Simulation and Molecular Docking of Spiro Pyrrolidine-2,3'-Thieno [2,3-d]Pyridazin-Hydrazide as Green Agricultural Product. *Polycyclic Aromatic Compounds*, 44(5), 2991–3008.

Rizk, S.A., El-Sayed, A.A., Mounier, M.M. 2017. Synthesis of Novel Pyrazole Derivatives as Antineoplastic Agent. *Journal of Heterocyclic Chemistry*, 54(6), pp. 3358–3371

Shalaby, M.A., BinSabt, M.H., Rizk, S.A., Fahim, A.M. 2024. Novel pyrazole and imidazolone compounds: synthesis, X-ray crystal structure with theoretical investigation of new pyrazole and imidazolone compounds anticipated insecticide's activities against targeting Plodia interpunctella and nilaparvatalugens. *RSC Advances*, 14(15), 10464–10480

Song, Z.; Liu, C.; Müller, K.; Yang, X.; Wu, Y.; Wang, H. 2018. Silicon regulation of soil organic carbon stabilization and its potential to mitigate climate change. Earth-Science Reviews, 185, 463-475

Tondera, K., Blecken, G., Tournebize, J., Viklander, M., Österlund, H.,Wikström, A.A., Tanner, Chris C, Tondera, K, Blecken, G.-T, Viklander, Á.M., Österlund, Á.H., Wikström, Á.A.A., Tournebize, J, Tanner, C. C. 2018. Emerging Contaminants:

Occurrence, Treatment Efficiency and Accumulation Under Varying Flows, 93–109. https://doi.org/10.1007/978-3-319-70013-7_6

Wang, J.L., Xu, L.J. 2011. Advanced Oxidation Processes for Wastewater Treatment: Formation of Hydroxyl Radical and Application, 42,251–325. https://doi.org/10.1080/10643389.2010.507698

Yu, G. H.; Chi, Z. L.; Teng, H. H.; Dong, H. L.; Kappler, A.; Gillings, M. R.; Polizzotto, M. L.; Liu, C. Q.; Zhu, Y. G. 2019. Fungus-initiated catalytic reactions at hyphal-mineral interfaces drive iron redox cycling and biomineralization. Geochimica et Cosmochimica Acta, 260, 192-203

Zare, K., Najafi, F., Sadegh, H. 2013. Studies of ab initio and Monte Carlo simulation on interaction of fluorouracil anticancer drug with carbon nanotube. J. Nanostruct. Chem., 3, 1–8.

Zare-Dorabei, R., Ferdowsi, S.M., Barzin, A., Tadjarodi, A. 2016. Highly efficient simultaneous ultrasonic-assisted adsorption of Pb (II), Cd (II), Ni (II) and Cu (II) ions from aqueous solutions by graphene oxide modified with 2, 20 -dipyridylamine: central composite design optimization. Ultrason. Sonochem, 32, 265–276.

Zelmanov, G., Semiat, R. 2008. Phenol oxidation kinetics in water solution using iron (3)-oxide-based nano-catalysts. Water Res., 42, 3848–3856.

Zhang, L., Huang, T., Zhang, M., Guo, X., Yuan, Z. 2008. Studies on the capability and behavior of adsorption of thallium on nanoAl_2O_3. J. Hazard. Mater., 157 (2), 352–357.